UCLA
UCLA Electronic Theses and Dissertations

Title
Power Efficiency of Piezoelectric Fan Cooling

Permalink
https://escholarship.org/uc/item/7t55h4hz

Author
Wang, Yide Wang

Publication Date
2017

Peer reviewed|Thesis/dissertation

eScholarship.org Powered by the California Digital Library
University of California

UNIVERSITY OF CALIFORNIA

Los Angeles

Power Efficiency of Piezoelectric Fan Cooling

A thesis submitted in partial fulfillment of the

requirements for the degree Master of Science

in Mechanical Engineering

by

Yide Wang

2017

© Copyright by

Yide Wang

2017

ABSTRACT OF THE THESIS

Power Efficiency of
Piezoelectric Fan Cooling

by

Yide Wang

Master of Science in Mechanical Engineering
University of California, Los Angeles, 2017
Professor Yongho Ju, Chair

Recent developments in electronic and optoelectronic devices, especially in the highly power-sensitive areas of portable and wearable applications, have led to increased challenges in their thermal management. Conventional rotary fans are difficult to scale down and power-inefficient when miniaturized. Piezoelectric fans, which typically consist of flexible blades mechanically fixed to piezoelectric actuators, are promising alternatives to rotary fans because they have simpler structures, produce less noise, and require less power consumption [1]. Although piezoelectric fans have been commercially available for over a decade, systematic study of their power consumption mechanism has been limited. A combined experimental and modeling study is conducted to help elucidate the mechanism of power dissipation in piezoelectric fans, and correlate them with heat transfer performance.

Powers consumed by a commercially available piezoelectric fan and by its piezoelectric actuator (with the fan blade cut off) are measured separately as a function of frequency and bias input voltage. A mechanical model is next developed to theoretically partition the fraction of power transferred to the surrounding air and that portion consumed by the piezoelectric actuator. In parallel, the heat transfer coefficients over a heated flat surface are measured for a set of piezoelectric fans of different blade lengths and thicknesses to obtain insight into piezoelectric fans' cooling enhancements normalized by power consumptions.

It is observed that the power consumption predicted by the proposed model for a piezoelectric actuator (with the blade cut off) agrees with that measured. In addition, the model estimated flow power (power transferred to surrounding air) matches the difference between the separately measured total power consumption of the piezoelectric fan and that of its piezoelectric actuator, indicating the validity of the proposed model in partitioning the power consumption of a complete piezoelectric fan. It is also confirmed that the heat transfer performance of the piezoelectric fan is closely related to its induced flow power rather than the total power consumed. As will be discussed in following chapters, the "power efficiency of piezoelectric fan cooling" should be characterized by its flow power rather than total power consumption.

The thesis of Yide Wang is approved.

Richard E.Wirz

Adrienne G. Lavine

Yongho Ju, Committee Chair

University of California, Los Angeles

2017

Table of Contents

Acknowledgements

Firstly, I would like to thank my advisor Professor Yongho Ju for his precious support and guidance throughout the project.

Secondly, I would like to thank Professor Wirz and Professor Lavine for being willing to serve as my committee members.

I would also like to acknowledge the contribution from Navid Dehdari Ebrahimi to the current work. Important discussions with Zezhi Zeng, Zhengxian Qu, and Chao Fan are appreciated.

Finally, I would like to extend special thanks to my family members for their love and support.

1. Introduction

A typical piezoelectric fan consists of a PZT (lead zirconate titanate) bimorph actuator attached to a flexible blade (usually made of polymers such as polyester, etc.). The PZT bimorph actuator is comprised of a thin metal shim sandwiched between two PZT layers. When applying a voltage with opposite polarities across two PZT layers, one layer expands while the other contracts, creating a bending moment that leads to the deflection of the actuator. By applying an AC voltage, the bimorph actuator starts to vibrate at the same frequency as that of the excitation voltage. It is usually set to vibrate at the fundamental resonance frequency of the blade, inducing a large vibration amplitude of the blade, to generate a relatively high net air flow in a forward direction, enhancing heat transfer from a variety of heat sources. Utilizing the resonance phenomenon without prominent loss mechanism, such as friction loss, a promising feature of piezoelectric fans is their significantly low power consumption compared to that of traditional rotary fans, which provide a similar heat transfer performance [2].

1.1 Objective

Usually, people operate piezoelectric fans under the first resonance frequency of the blade, with the optimization of the blades' geometrical shape or system configuration to obtain maximum cooling ability. However, it is observed that the power consumption of a piezoelectric fan can be very different when operating at frequencies offset from resonance, which can be achieved by either modifying the geometry of the fan blade or adjusting the frequency of the excitation voltage. Since recent developments in portable electronics have made them more power-sensitive due to limited battery capacity, a geometrically or

systematically optimized piezoelectric fan may not necessarily be power efficient, in terms of cooling ability normalized by its power consumption. The principal existing studies have not systematically considered power consumption, considering the frequency dependence and detailed power dissipation partitioning between that dissipated through the PZT actuator and that through the fan blade. In the current work, the power consumption of the piezoelectric fan is studied both experimentally and theoretically. It is believed that the total power consumption of piezoelectric fan is the summation of the PZT actuator's internal power dissipation and the flow power of the surrounding air provided by the vibrating fan blade. The voltage and current going through the piezoelectric fan are recorded and processed to experimentally determine the total power. The internal dissipation of a solo PZT actuator, the so-called "parasitic power dissipation" which always exists but does not contribute to fan cooling performance, is both theoretically estimated and experimentally measured. A two-degree of freedom mass-spring-damper system (MSD) is proposed to represent the piezoelectric fan and to estimate the flow power by experimentally obtaining the aerodynamic damping coefficient of the fan blade.

While the model predicting the power consumption of a piezoelectric fan is developed, as discussed in chapter two, multiple experiments are conducted simultaneously, studying the cooling enhancement provided by the piezoelectric fan over a flat surface to discover the power efficiency of cooling. Natural convection, forced convection, and radiation are the dominant energy transfer modes [3]. By heating up the test surface to a certain temperature, natural convection and radiation effect are characterized by knowing the steady state temperature and input power of the heat source. The piezoelectric fan is then turned on to impose forced convection. After reaching a steady state again, the forced

convection coefficient is obtained by knowing the input heat source power and final temperature difference. The heat transfer enhancement, in terms of the forced convection coefficient, can then be normalized by the piezoelectric fan's flow power, determining the power efficiency of piezoelectric fan cooling. Chapter three will discuss the reasons that such power efficiency should be determined by using flow power.

1.2 Literature Review

The fluid dynamics and cooling performance of piezoelectric fans and, more generally, vibrating cantilever beams have been extensively studied in the past few decades. Kim et al. [4] investigated and visualized the flow field generation in the air produced by piezoelectric fans using "Particle Image Velocimetry (PIV)" and a "smoke visualization technique". They observed that during each vibration cycle, a pair of counter-rotating vortices is generated. These two vortices induce a high-velocity region in between them, in which the maximum velocity is nearly four times the maximum speed of the tip of the plate.

Eastman et al. [5] investigated the thrust generated due to the motion of a piezoelectrically actuated oscillating cantilever over a wide range of Reynolds numbers and proposed a correlation relating the thrust to the vibration amplitude.

Acikalin et al. [6] found that the cooling performance of a piezoelectric fan, in terms of convective heat transfer coefficient, is affected by several parameters, such as fan tip distance to heat source, vibrating frequency, amplitude ratio at resonance, etc. In their work, a transfer function including all parameters is introduced to predict the convective heat transfer coefficient. They also experimentally visualized the induced flow, determined the optimum

relative position between fan and heat source, and implemented the piezoelectric fan as a cooling device into commercially available electronics.

Kimber et al. [7] constructed the pressure-flowrate relationship (commonly known as the fan curve) for the piezoelectric fan. Inspired by AMCA standard 210, with some modification to the experimental setup, they managed to measure the differential pressure and flow rate induced by two types of piezoelectric fans with steel and Mylar blades. It is observed that the stiffer fan blade has a higher resonance frequency and smaller vibration amplitude than those of the softer blade, leading to a higher static pressure but lower flow rate. It is also concluded that the flow rate is in the order of frequency multiplied by amplitude square.

Wait et al. [8] studied the electromechanical coupling factors (EMCF) of a piezoelectric fan operating at 1^{st} to 4^{th} resonance frequencies. The EMCF represents the efficiency of the fan in converting electrical energy to mechanical energy. It is concluded that the piezoelectric fan has the highest EMCF operating at the 1^{st} natural frequency. More importantly, Wait mentioned the power consumption and energy losses through operation. Regarding the piezoelectric fan as an electrical component, the power consumption can be obtained by integrating the product of input voltage and current through the time of one vibration cycle and multiplying the frequency. To theoretically prove the validity of such a measurement, an equivalent RLC circuit is proposed to represent the piezoelectric fan, where the power consumption is directly related to the circuit impedance. However, no actual values of resistor, inductor, and capacitor are determined except the measured power.

During the 1990s, Liang et al. [9] developed an impedance method for PZT-actuated beam vibration, incorporating the mechanical properties of the system into the expression of

electrical impedance to obtain electrical power consumption. According to Liang, the power consumption of a PZT actuator consists of dielectric loss in the PZT actuator, heat dissipation, and mechanical power dissipated in the host structure. However, one of the key assumptions of the original impedance method is that the piezoelectric actuator is negligibly small compared to the host structure, providing point driving force whereas, in the piezoelectric fan system, the piezoelectric actuator becomes the dominant component affecting the dynamic response.

Based on Liang's work, Cho et al. [10] developed a five-port equivalent electric circuit, where the electrical portion of a PZT bimorph actuator power losses is represented by electrically equivalent impedance. The electrically dissipated power in the PZT actuator can then be obtained by knowing the input voltage and the real part of its equivalent impedance. However, interface bonding material affects the vibration of the PZT actuator and also imposes internal frictional dissipation, based on the experimental results shown in later sections. Sheu et al. [11] studied the influence of bonding glues on the vibration of piezoelectric fans. By attaching the blade to a PZT actuator using different thicknesses of either black epoxy or RTV silica gel glues, they experimentally obtained different vibrational amplitudes of a fan blade at the fan blade's resonance frequencies. They observed that the vibrational amplitude of the blade decreases as the thickness of the glue increases.

From the literature review, it is important to realize that, since a piezoelectric fan converts electrical energy into mechanical energy, its driving power needs to be dissipated through the actuator, which serves as an electrical component, and through the mechanical vibration of both the actuator and the fan blade. Therefore, chapter two will demonstrate models that predict such electrical and mechanical power dissipation.

2. Model of Piezoelectric Fan Power Consumption

2.1 PZT Actuator Internal Dissipation (Parasitic Power Dissipation)

Since the vibrating PZT actuator is an electromechanical conversion device, two major portions, mechanical dissipation and dielectric dissipation, compose its power consumption. As an electrical component, electrical charges transport through the piezoelectric ceramics, experiencing resistance while changing direction at each half-cycle under an alternating electric field [12].

As mentioned in the introduction, Sheu et al. [11] observed that different interface bonding materials affect the vibrational dynamic response of the piezoelectric fan by imposing various mechanical damping. Therefore, it is believed that, for a three-layer bimorph actuator, the mechanical dissipation caused by the shear motion of its internal viscoelastic layers needs to be taken into consideration.

The current chapter will present the development of models that estimate both dielectric loss and mechanical loss through the actuator. The summation of these two losses is believed to be the total power dissipation of the PZT actuator.

2.1.1 Mechanical loss

To characterize the vibrating dynamics response of a piezoelectric fan, Yao and Uchino [13] modeled it as a two-degree of freedom (DOF) MSD, where the PZT actuator and fan blade are represented by two 1 DOF systems with their own lumped mass, spring constant, and damping coefficient connected together by a spring. Their damping mechanisms are modeled as linear velocity damping where the damping force equals the

damping coefficient multiplied by the velocity. With damping coefficients and spring constants of both components known, the equation of motion (EOM), which is a second order non-homogeneous differential equation, can be solved to obtain the vibration amplitudes of both the blade and the PZT actuator under various frequencies. However, our measured amplitudes of the PZT actuator show a slight difference from those predicted by their proposed model. Fig. 1 shows the measured amplitudes of the PZT actuator's tip, $|Y|$, normalized by its static deflection, δ_{static}, under multiple input voltage levels plotted versus frequency up to resonance proximity. The static deflection represents the bending deflection of the actuator tip under static input voltage, or an AC voltage with zero frequency. By iteratively adjusting the damping coefficient of the PZT actuator, C_1, the resulting actuator tip deflections are compared with measured ones. The best match is shown on the graph by a dashed line with $C_1 = 0.3$.

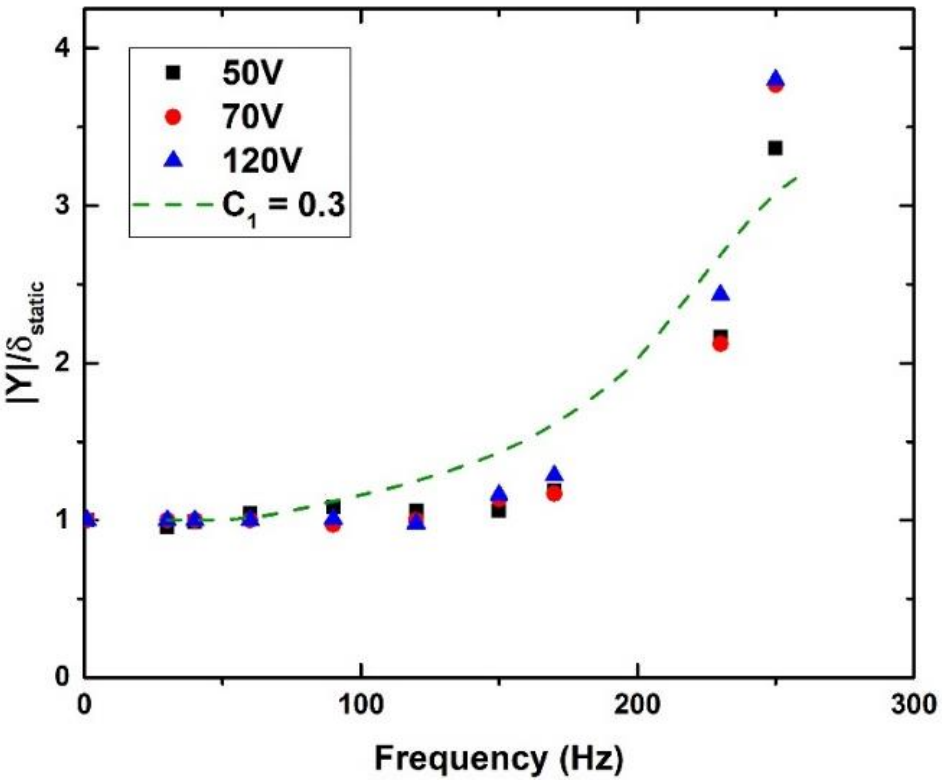

Fig. 1. measured actuator vibration amplitudes compared with predicted ones

As seen in Fig. 1, the measured vibration amplitudes show a steeper increase when approaching resonance, demonstrating the inaccuracy in the modeling of the damping mechanism. The following section presents a proposed modification in the modeling damping mechanism.

Low and Gou [14] state that although a simple two-layer piezoelectric actuator can be modeled by a linearly damped mass-spring model, the presence of a metal shim in between (and additional layers of bonding material) affects the motion of the tip. They developed a vibrational model in which they added a new "state variable" to the equation of motion to account for stress hysteresis due to strain residual which exists in a vibrating beam. Here, we utilize their model with some simplifications, as explained below, to estimate the power

consumption of PZT bimorph. Fig. 2 shows the MSD system representation of the PZT actuator.

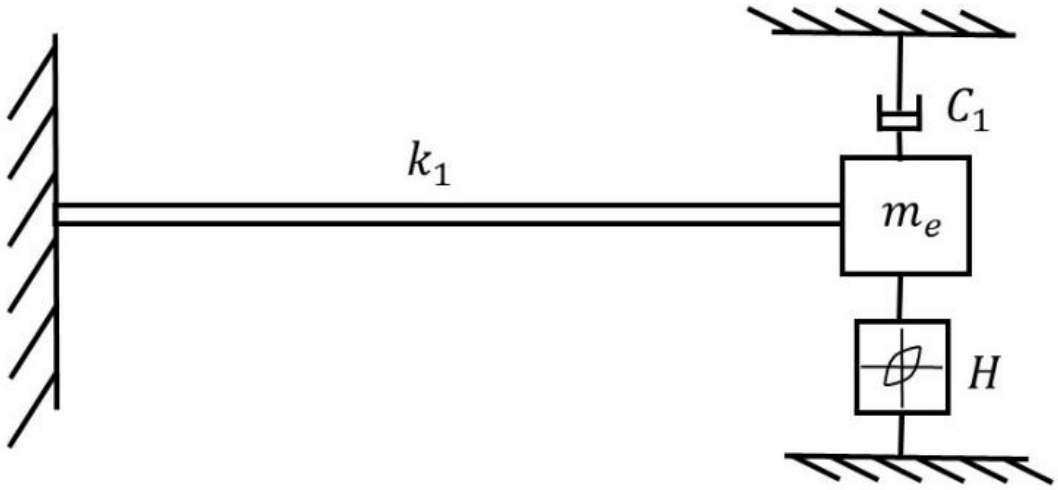

Fig. 2. One DOF mass spring damper system

Instead of solving only the EOM (Eq. 2), an additional equation relating the state variable, z (representing hysteresis), to the excitation voltage (Eq. 1) also needs to be solved.

$$\dot{z} = \alpha d_e \dot{V} - \beta|\dot{V}|z - \gamma\dot{V}|z| \tag{1}$$

$$m_{e1}\ddot{y} + C_1\dot{y} + k_1 y = k_1(d_e V - z) \tag{2}$$

α, β and γ are parameters that define the shape of the hysteresis loop. m_{e1} is the effective mass of the PZT actuator. Since the vibration amplitude of the PZT actuator is small compared to its length and width, it can be modeled as a rigid cantilever beam with the effective mass $m_{e,1} = \frac{33}{140} m_{10}$, where m_{10} is the original mass of the PZT actuator, being

located at the tip of the actuator. $k_1$is the stiffness of the PZT actuator, which can be obtained by measuring the resonance frequency and substituting in $2\pi f_{resonance} = \sqrt{\frac{k_1}{m_{e1}}}$. d_e is the effective piezoelectric coefficient relating the voltage applied to the actuator to the displacement of the tip.

Since Eq. 1 is not coupled with Eq. 2, it can be solved independently. Fig. 3 shows the results for the different choices of α, β, and γ.

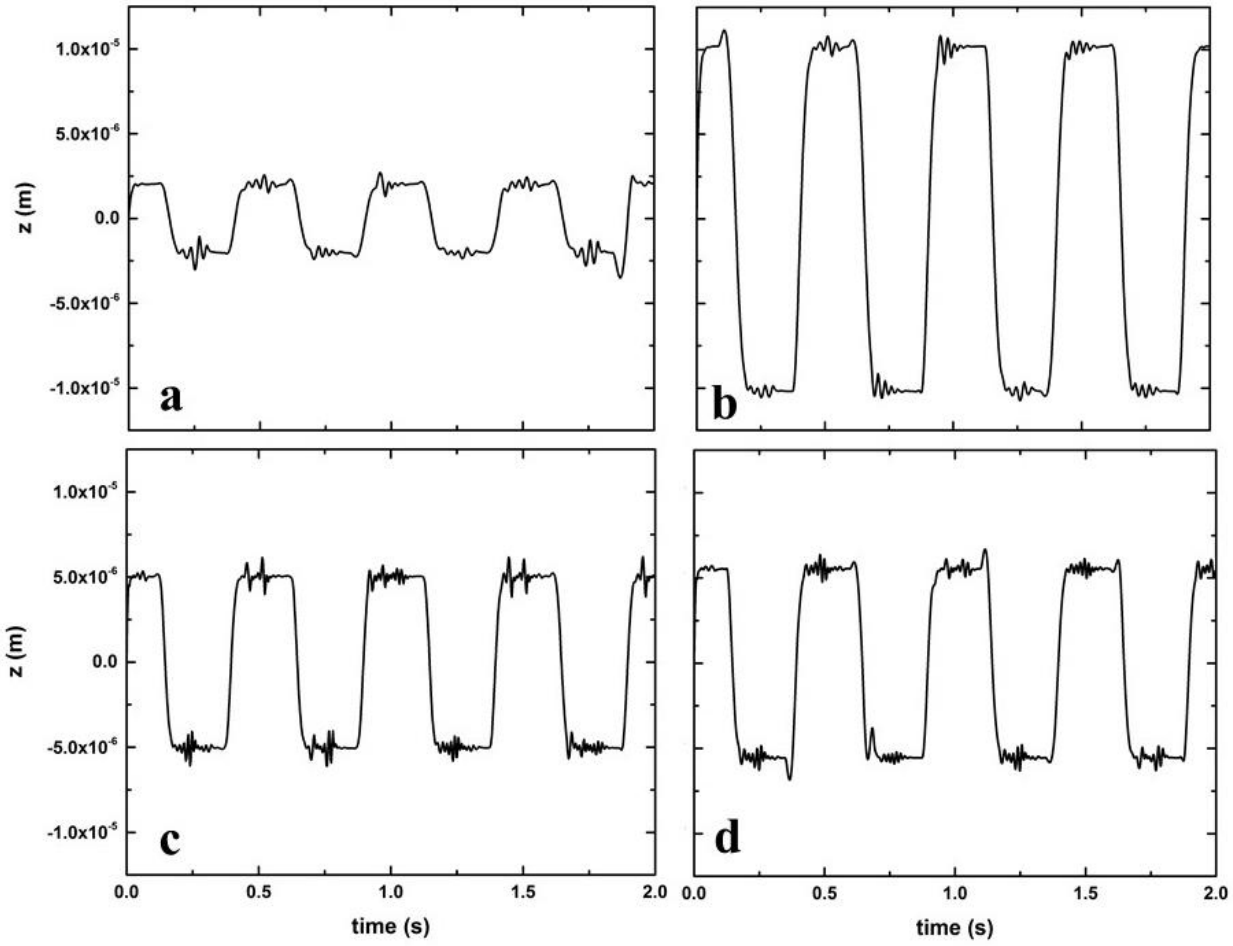

Fig. 3. Time dependent state variable z with different choice of *α, β* and *γ*. a) $\alpha=1\times10^{-1}$, $\beta=5\times10^{-2}$, $\gamma=-1\times10^{-3}$, $d_e=1\times10^{-6}$ b) $\alpha=5\times10^{-1}$, $\beta=5\times10^{-2}$, $\gamma=-1\times10^{-3}$, $d_e=1\times10^{-6}$ c) $\alpha=5\times10^{-1}$, $\beta=1\times10^{-1}$, $\gamma=-1\times10^{-3}$, $d_e=1\times10^{-6}$ d) $\alpha=5\times10^{-1}$, $\beta=1\times10^{-1}$, $\gamma=-1\times10^{-2}$, $d_e=1\times10^{-6}$

As can be observed, *z* acts as a constant value parameter whose sign is changing with velocity. Therefore, Eq. 2 can be simplified to:

$$m_e\ddot{y} + C_1\dot{y} + k_1 y + H\ sign\ (\dot{y}) = F_0 \sin(\omega t) \tag{3}$$

$k_1 d_e V$ is substituted with its equivalent force on the tip (F_0) and $k_1 z$ is replaced with $H\ sign(\dot{y})$. Two unknowns are present in this equation, (C_1 and H).

Eq. 3 is the new EOM of the actuator that can be used to iteratively estimate C_1 and H by fitting the resulting tip deflections with those measured.

By knowing C_1 and H, the mechanical power dissipation of the solo PZT actuator can then be calculated using the following expression:

$$P_{PZT,mech} = 4H|Y| + \pi C_1 \omega |Y|^2 f \tag{4}$$

2.1.2 Dielectric loss from PZT actuator

Besides mechanical dissipation through vibration, as an electrical component, dielectric loss through a PZT actuator also contributes a significant portion, along with mechanical loss.

Based on the five-port equivalent electric circuit developed by Cho et al. [10], the PZT actuator is represented by an equivalent electrical circuit whose electrical and mechanical aspects are both represented by electrically equivalent impedance. The dissipative

power in the PZT actuator can then be obtained by knowing the input voltage and the real part of its equivalent impedance.

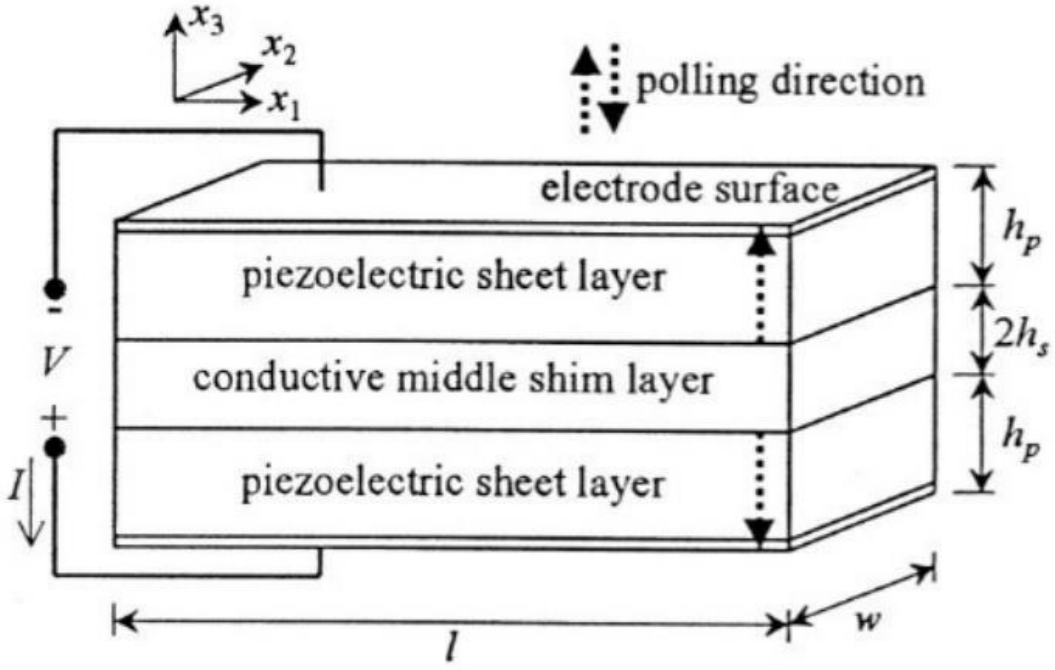

Fig. 4.[10] Three-layered PZT bimorph actuator

Eq. 5 is the piezoelectric constituent equation, describing the axial strain of a PZT actuator under the electric field *E*.

$$\varepsilon_{p_1} = S_{p_{11}}^{E} \sigma_{p_1} + d_{31} E_3 \tag{5}$$

Based on Eq. 5, the dielectric displacement can be derived as

$$D_3 = d_{31} \sigma_{p_1} + p_{33}^{\sigma} E_3 \tag{6}$$

where ε and σ denote strain and stress respectively. *S* is the mechanical compliance modulus, *d* is the piezoelectric strain constant, *E* represents the electric field across the PZT actuator, and p denotes the dielectric constant, also known as primitivity. Superscript *E* and σ mean

constant electric field and constant stress condition respectively. Subscript *p*, *s*, and *b* represent the piezoelectric layer, metal shim layer, and entire bimorph actuator respectively.

By modeling the PZT actuator as a cantilever beam under free vibration, the EOM can be obtained from the Euler-Bernoulli beam theory:

$$\overline{K_b}\frac{\partial^4 u_3}{\partial x_1^4} + \overline{\rho_b}\frac{\partial^2 u_3}{\partial t^2} = 0 \tag{7}$$

In the EOM, $\overline{K_b}$ is the effective bending rigidity, defined as

$$\overline{K_b} = \frac{2}{3}w\left[\frac{1}{S_{p_{11}}^E}\left(\left(h_p + h_s\right)^3 - h_s^3\right) + \frac{1}{S_{s_{11}}}h_s^3\right] \tag{8}$$

and $\overline{\rho_b}$ is the density, determined as follows:

$$\overline{\rho_b} = 2w(\rho_p h_p + \rho_s h_s) \tag{9}$$

The solution of the EOM is in the form of

$$u_3 = [\alpha_1 \cos(\lambda_b x_1) + \alpha_2 \sin(\lambda_b x_1) + \alpha_3 \cosh(\lambda_b x_1) + \alpha_4 \sinh(\lambda_b x_1)]e^{j\omega t} \tag{10}$$

where $\alpha_1 - \alpha_4$ are coefficients and λ_b is a constant, expressed as

$$\lambda_b = \left(\frac{\overline{\rho_b}}{\overline{K_b}}\omega^2\right)^{\frac{1}{4}} \tag{11}$$

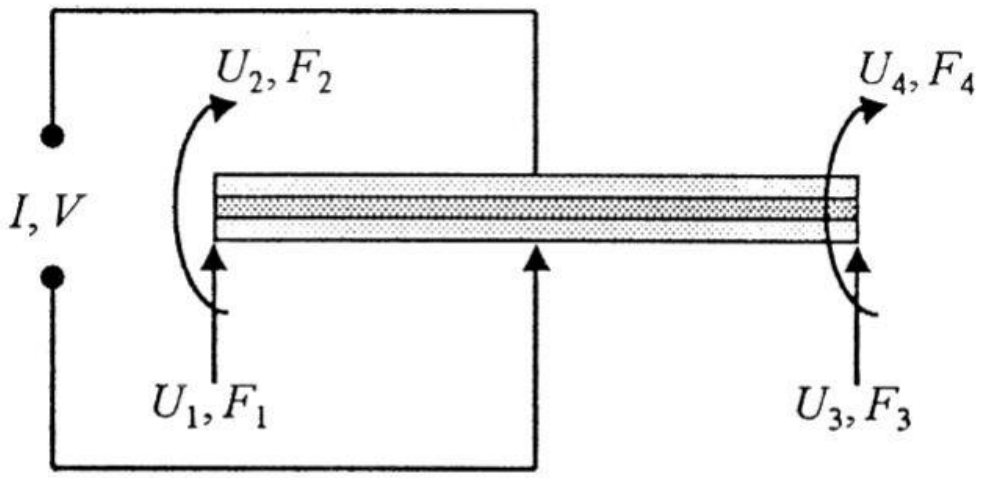

Fig. 5. [10] Flows (U_i, I) and efforts (F_i, V) of PZT bimorph actuator

In the equivalent circuit of bending motion, the bending moment and transverse shear force are defined as mechanical efforts. The mechanical efforts are then expressed as vertical and rotational displacement, defined as mechanical flow. The electric flow is expressed in terms of mechanical flow and voltage:

$$I = -N(U_2 - U_4) + j\omega C_c V \tag{12}$$

The linear relationship between flows and efforts is expressed by a 5×5 impedance matrix:

$$\begin{Bmatrix} F_1 \\ F_2 \\ F_3 \\ F_4 \\ V \end{Bmatrix} = \begin{bmatrix} Z_{11} & Z_{12} & Z_{13} & Z_{14} & Z_{15} \\ & Z_{22} & Z_{23} & Z_{24} & Z_{25} \\ & & Z_{33} & Z_{34} & Z_{35} \\ & \text{Symm} & & Z_{44} & Z_{45} \\ & & & & Z_{55} \end{bmatrix} \begin{Bmatrix} U_1 \\ U_2 \\ U_3 \\ U_4 \\ I \end{Bmatrix} \tag{13}$$

Boundary conditions for a clamped-free ends cantilever beam are

$$U_1 = U_2 = 0, F_3 = F_4 = 0 \tag{14}$$

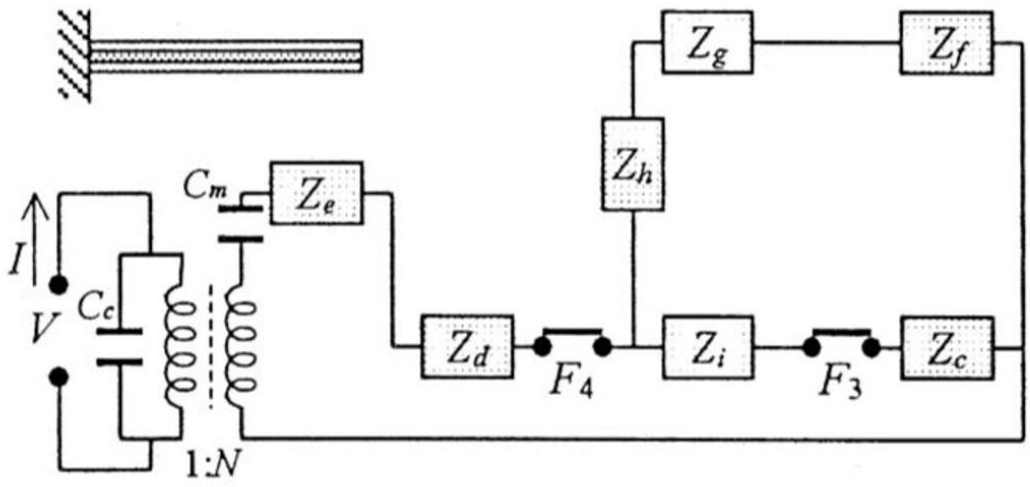

Fig. 6. [10] Equivalent circuit of a clamped-free ends cantilever beam

The admittance Y of such a circuit is

$$Y = j\omega\left(C_c + \frac{N^2}{\overline{K_b}\lambda_b}\frac{-cn-sm}{1+cm}\right) \tag{15}$$

where

$$c = \cos(\lambda_b l), s = \sin(\lambda_b l), m = \cosh(\lambda_b l), n = \sinh(\lambda_b l) \tag{16}$$

$$N = -\frac{d_{31}}{S^E_{P_{11}}} w\left(\frac{h_p+2h_s}{2}\right) \tag{17}$$

In Eq. 15, ω is the angular vibration frequency. C_c denotes a capacitance, defined as

$$C_c = \frac{p^\sigma_{33}\left(1-\frac{d^2_{31}}{S^E_{p_{11}}p^\sigma_{33}}\right)lw}{2h_p} \tag{18}$$

The dielectric power dissipation can then be obtained knowing the input voltage and the real part of its admittance:

$$P_{PZT,dielectric} = \frac{V^2}{2} Re(Y) \tag{19}$$

Finally, by accounting for the mechanical loss through viscoelastic layers due to vibration and dielectric loss, the total power dissipation of a PZT actuator can be found by summing up the two parts discussed above.

$$P_{PZT,total} = P_{PZT,dielectric} + P_{PZT,Mech} \tag{20}$$

2.2 Flow Power Estimation

As discussed in previous sections, besides the power consumed by the PZT actuator, the other significant portion of consumed input power dissipates through the fan blade into the surrounding air as flow power. To estimate the flow power, the piezoelectric fan is represented by an MSD system with two DOF, as shown below [13]:

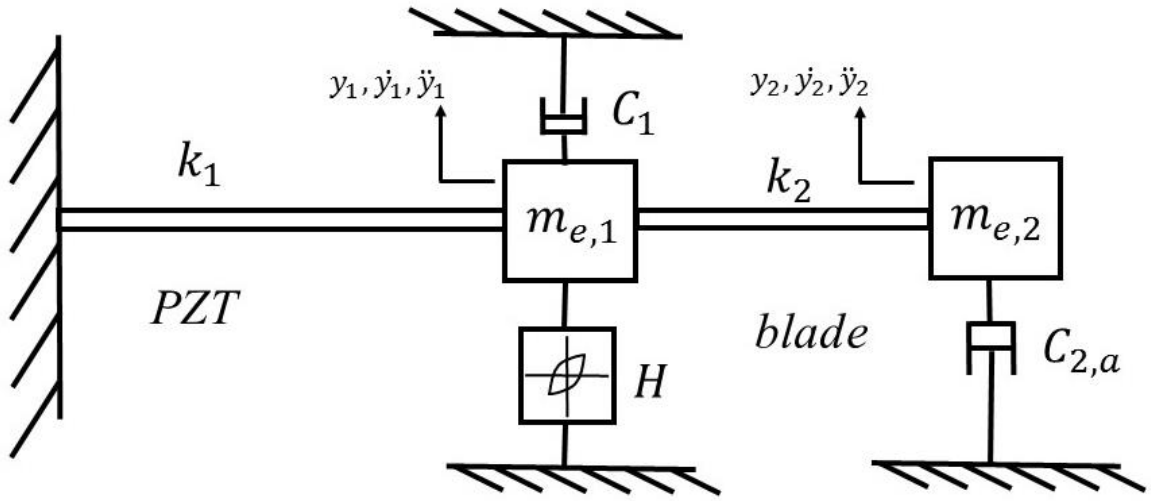

Fig. 7. Lumped mass-spring-damper model of piezoelectric fan

The EOM of the whole system, which consists of two-second order differential equations, can be written in matrix form as:

$$\begin{bmatrix} m_{e,1} & 0 \\ 0 & m_{e,2} \end{bmatrix} \begin{bmatrix} \ddot{y}_1 \\ \ddot{y}_2 \end{bmatrix} + \begin{bmatrix} C_1 & 0 \\ 0 & 0 \end{bmatrix} \begin{bmatrix} \dot{y}_1 \\ \dot{y}_2 \end{bmatrix} + \begin{bmatrix} 0 & 0 \\ 0 & C_{2,a} \end{bmatrix} \begin{bmatrix} \dot{y}_1 |\dot{y}_1| \\ \dot{y}_2 |\dot{y}_2| \end{bmatrix}$$

$$+ \begin{bmatrix} H & 0 \\ 0 & 0 \end{bmatrix} sign\left(\begin{bmatrix} \dot{y}_1 \\ \dot{y}_2 \end{bmatrix} \right) + \begin{bmatrix} (K_1 + k_2) & -K_2 \\ -K_2 & K_2 \end{bmatrix} \begin{bmatrix} y_1 \\ y_2 \end{bmatrix} = \begin{bmatrix} F_0 \sin(\omega t) \\ 0 \end{bmatrix} \quad (21)$$

$m_{e,1}$ and $m_{e,2}$ are the effective mass of the PZT actuator and blade. Since the blade has a comparable vibration amplitude to its dimensions, it is modeled as follows [15]:

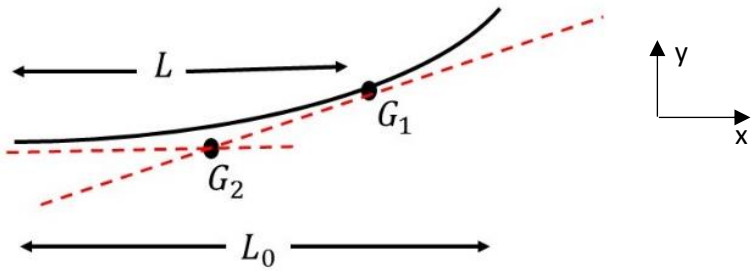

Fig. 8. [15] Original deformation of blade

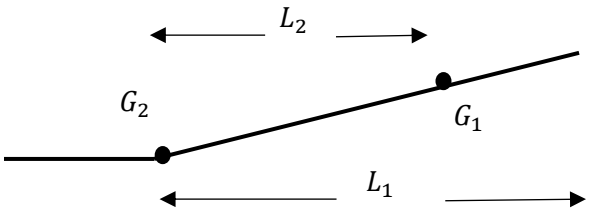

Fig. 9. [15] Modified deformation of blade

The blade has an original length of L_o , an original mass m_{20}, and a lumped mass m_2 located at point G_1 with a distance L from the fixed wall. When vibrating, the center of mass G_1 rotates around point G_2. G_2 is the intersection of the equilibrium plane and the tangential line of point G_1. The functional expression of the original blade deformation is

$$y(x) = a(3Lx^2 - x^3) \tag{22}$$

Distance L is determined by the average of axial position weighted by the distributed inertia force:

$$L = \frac{\omega^2 \int_0^{L_0} x\rho_p Why(x)dx}{\omega^2 \int_0^{L_0} \rho_p Why(x)dx} = 0.7236L_0 \tag{23}$$

ρ_p is the density of the blade's material, and W and h are the blade's width and thickness respectively.

The effectively lumped mass of a vibrating blade can be determined by equating the distributed inertial force to the force acting at point G_1:

$$m_2\omega^2 y(L) = \omega^2 \int_0^{L_0} \rho_p Why(x)dx \tag{24}$$

$$m_{e,2} = 0.625m_{20}$$

The EMO is solved iteratively to find C_{2a}, with all parameters related to the PZT actuator known from the previous section. The solution of y_2 closely matches the measured blade amplitude, being within 0.02 mm of error. All blade amplitudes in the operational frequency range are obtained and plotted with measured values. With C_{2a} being determined at around 0.0011, the flow power is obtained as follows [16]:

$$P_f = \frac{8}{3} C_{2a} |y_2|^3 \omega^2 f \tag{25}$$

ω and f denote the angular frequency and frequency respectively.

Finally, based on the flow power estimation model and PZT actuator power consumption discussed in the previous section, the total power of a piezoelectric fan can be found as the summation of mechanical loss and dielectric loss through a PZT actuator and the flow power of the surrounding air induced by the vibration of the fan blade:

$$P_{total} = \frac{8}{3} C_{2a} |y_2|^3 \omega^2 f + 4H|Y| + \pi C_1 \omega |Y|^2 + f \frac{V^2}{2} Re(Y) \tag{26}$$

2.3 Experimental Setup

The experimental study of a piezoelectric fan's power consumption mainly consists of two parts, power measuring and vibration amplitude measuring. As discussed in the previous section, the piezoelectric fan serves as an electrical component which converts electrical energy into mechanical energy. Therefore, to measure its electrical driving power, the alternating driving voltage and induced current need to be measured.

The power measurement setup consists of a function generator (Agilent 33220A), generating small amplitude (0.4V - 2V) pure sinusoidal voltage signals. Since the amplitude of the voltage is too small to directly drive the piezoelectric fan, an amplifier (TREK PZD700A) is connected in series to increase the amplitude by a factor of 100.

Fig. 10. Power measurement devices

The voltage and current crossing through a piezoelectric fan can be monitored and recorded by the LabVIEW [17] VI and processed by a MATLAB [18] script using the following equation to obtain measured power:

$$P_{total} = \frac{1}{T}\int_0^T V(t)I(t)\,dt \tag{27}$$

The LabVIEW VI samples both voltage and current signals at 5000 Hz. Sampled data points are fitted by a sine wave using the least square method; the resulting fitted sine waves of voltage and current are discretized into 5000 data points and integrated numerically to obtain power.

It is observed in the previous sections that predicting both the power dissipation in a PZT actuator and flow power are highly dependent on amplitude fitting to determine factors such as H and C_{2a}. Therefore, the other part of the experimental setup is built taking into consideration accurate amplitude measuring under high-frequency vibration.

Given the PZT actuator's small vibration amplitude and high-frequency vibration, a high-speed camera (capable of recording up to 16000 fps) is used, with a microscope attached to provide a satisfactory resolution. The resolution of measurements is 14 μm (~ 4% of the total displacement of the PZT actuator). A scaling ruler is located with a minimum distance from the point of interest in order to minimize any error due to perspective effects.

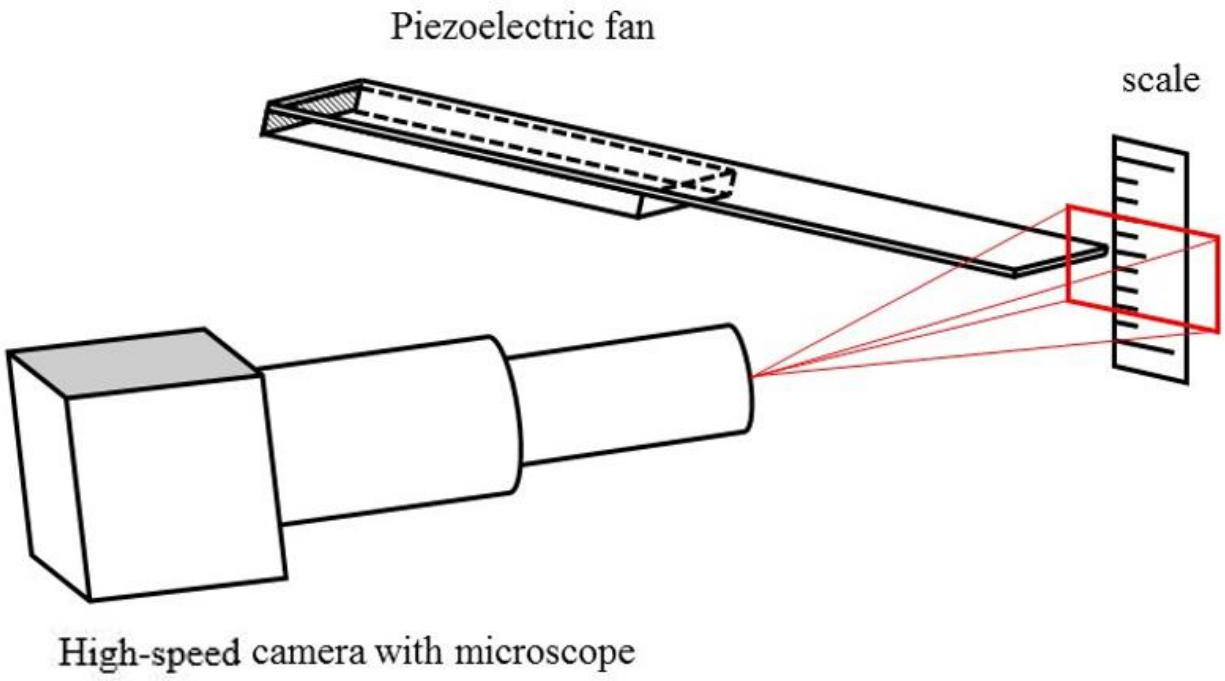

Fig.11. Experimental setup of amplitude measuring

The only difference between the experimental setup of a PZT actuator and that of a fan blade is the use of a regular lens instead of a microscope. With an amplitude ranging from 3 mm to 9 mm, the regular camera lens provides enough resolution, 0.11 mm, for the measurement uncertainty not to affect the result significantly.

ImagJ [19], a commercially available picture processing software, is used to measure the vibration amplitude by counting the number of pixels between two pixels that are showing the same location on a piezoelectric actuator or fan blade at two time-steps.

2.4 Results

In the following section, all results, including specific values for C_1, H, and C_{2a}, the power consumption of the PZT actuator, flow power, and power consumption of a complete piezoelectric fan, will be presented. Each type of model-predicted power consumption will be plotted along with the measured one to demonstrate the validity of the proposed model.

2.4.1 Fitting the amplitude of a PZT actuator and obtaining C_1 and H

To obtain C_1 and H for the first model, the tip amplitude of the piezoelectric actuator is measured at different frequencies (up to resonance) and bias voltages. A genetic algorithm [20] is then used to minimize the error between the model and measured data, and, finally, the best fit is found. Fig. 12 shows the measured amplitudes for three different voltages (50V, 70V, and 120V) along with the curve fittings obtained through the genetic algorithm (dashed lines). It is observed that the curve fitting process is not sensitive to the value of C_1, meaning that changing the value of C_1 in a wide range does not affect the quality of curve fitting. On the other hand, any small changes to H result in a noticeable deviation from the measured data points. C_1 has a rather fixed value of 0.01; however, the value of H changes almost linearly with the applied voltage (Fig. 13).

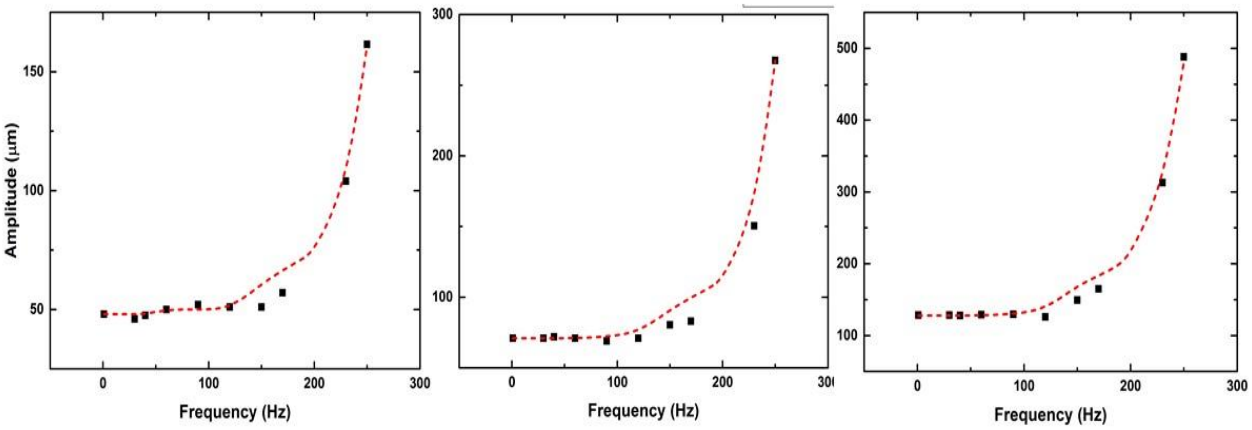

Fig. 12. Amplitude fitting of PZT actuator (From left to right: 50V, 70V, 120V)

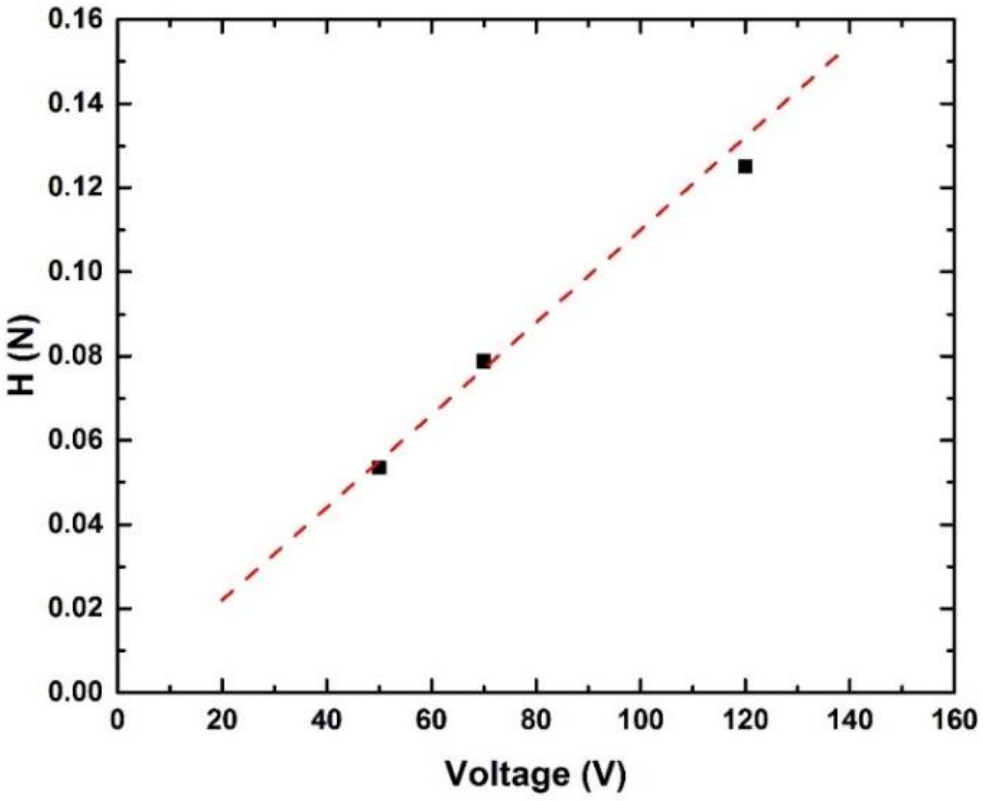

Fig.13. Voltage dependency of fitted H

The measured and predicted PZT actuator power consumptions, using Eq. 20, are shown in Fig. 14. It is observed that, for a fixed voltage, the power consumption in the PZT actuator increases linearly with frequency because the dominant parts of the power dissipation (mechanical loss and dielectric loss) have a linear dependence on the frequency. For lower voltages (60 V in Fig. 14), the dielectric loss is negligible, due to the small values of dielectric dissipation factor in a low electrical field [21] [22]. However, as the voltage increases, a larger portion of the total power is dissipated electrically (80 V and 100 V). A close agreement between the measured and predicted power consumptions demonstrates the validity of the proposed model.

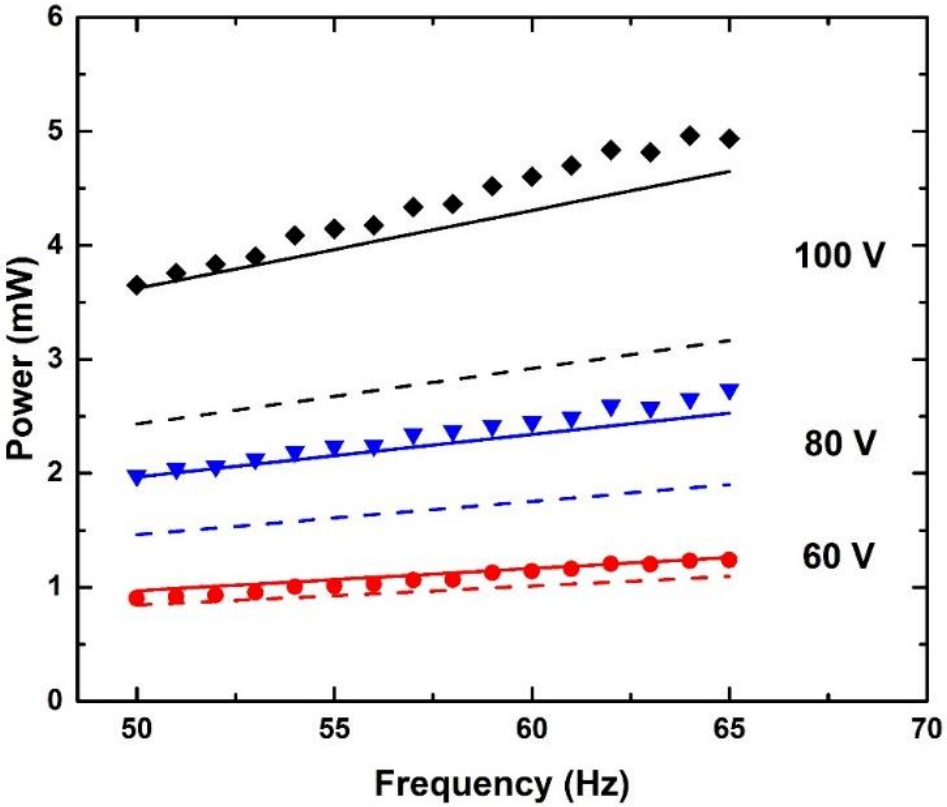

Fig. 14. The power consumption of a solo PZT actuator with different applied voltages: 60 V (red), 80 V (blue), and 100 V (green). (Measured powers are shown as data points; mechanical loss is presented with dashed-point lines, and the summation of mechanical and dielectric losses is depicted by solid lines.)

2.4.2 Fitting the amplitude of the blade and obtaining C_{2a}

The displacement of point G1 on the blade is measured and plotted, superimposed on the amplitude curve predicted by solving the EOM. The measured blade amplitudes, under working frequency range, match those predicted when $C_{2a} = 0.0011$

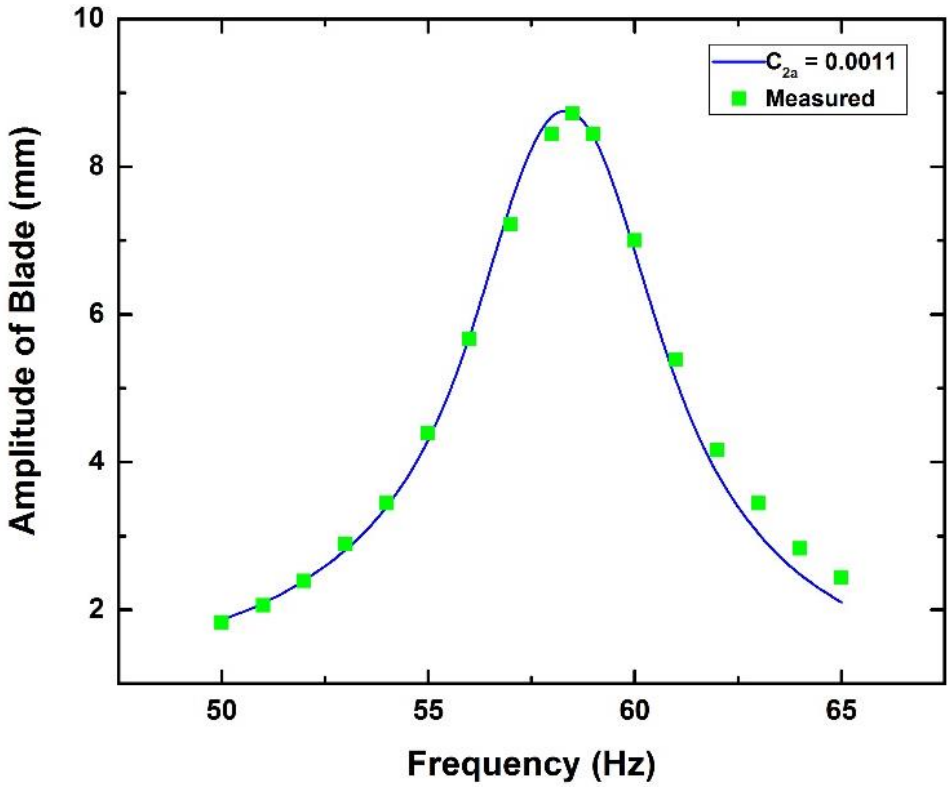

Fig.15. Measured and predicted fan blade amplitude with $C_{2a} = 0.0011$

The flow power is then calculated using Eq. 25 and the results are presented in Fig. 16. As expected, for a fixed voltage input, the flow power peaks at the resonance frequency, because its largest vibration amplitude transmits the maximum power to the surrounding air, while it approaches zero at off-resonance frequencies due to a rapid decrease in the amplitude. Since the vibration amplitude also depends on the voltage input, the flow power difference between different voltage inputs can also be explained by different vibration amplitudes of the blade.

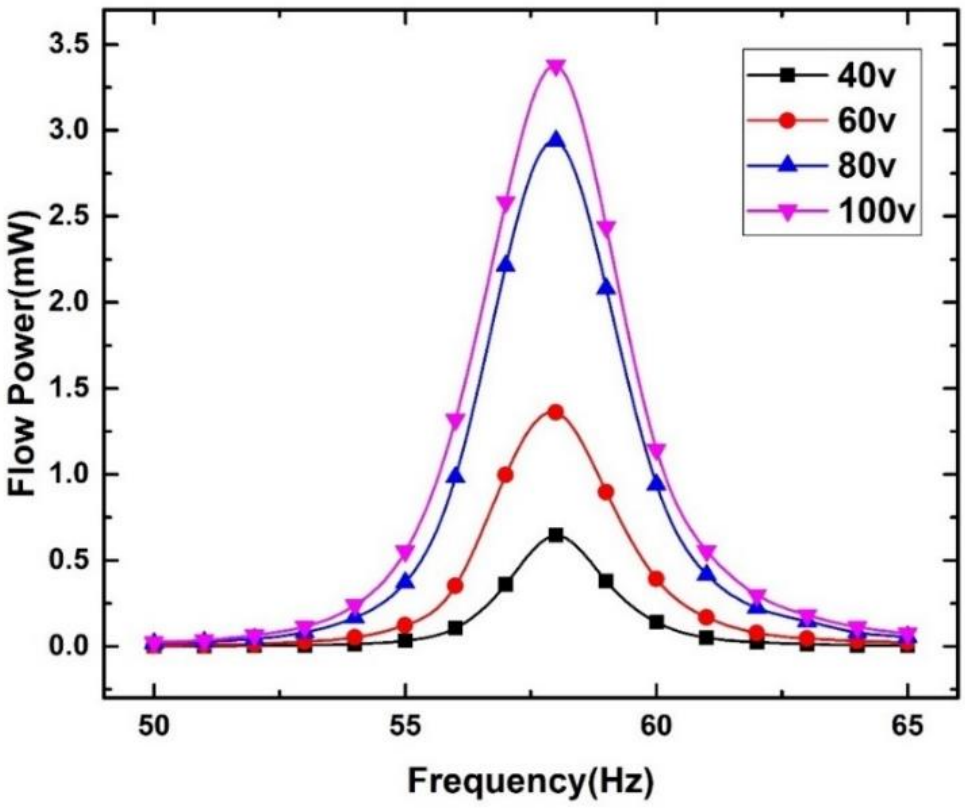

Fig.16. Predicted flow power of fan blade

2.4.3 Comparison of measured total power and predicted total power

A complete set of power partitioning for a piezoelectric fan operating at a fixed voltage (80 V), within the fan blade's resonance frequency proximity, is shown in Fig. 17. It is seen that at off-resonance frequencies, the presence of the fan blade has a minor impact on the power consumption. However, when operating near resonance frequency, 58Hz, a peak is observed in the total power consumption, believed to be the increasing power transfer to the surrounding air due to a rapid increase in the blade's vibration amplitude. Also, when comparing the measured total power consumption of a piezoelectric fan with the predicted flow power, it can be seen that there is a finite difference between these two curves that is equal to the measured power consumption of the PZT actuator.

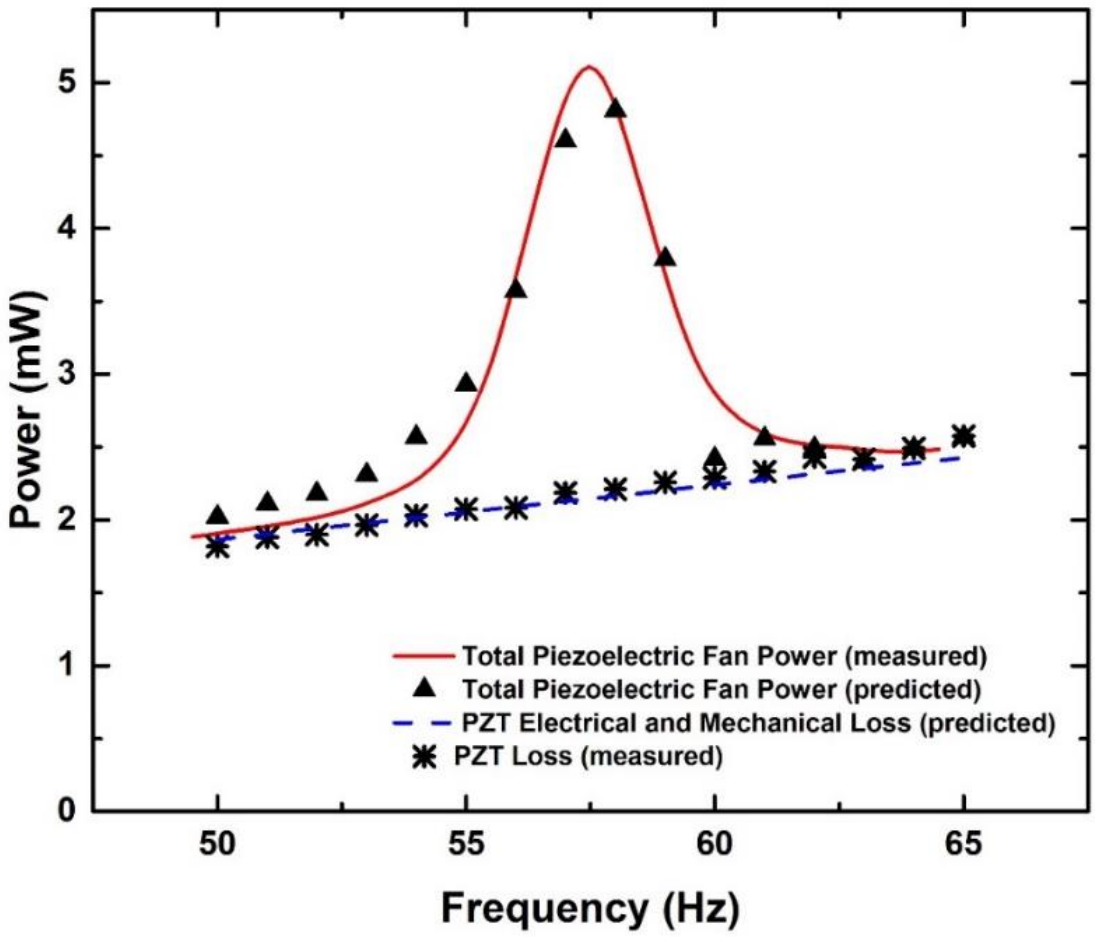

Fig.17. Power partitioning for a piezoelectric fan applied to 80 V.

The above plot shows that the predicted total power (red solid line), obtained from summing up the predicted flow power (purple solid line) and the predicted solo PZT actuator power (blue dashed-dot line), fits well with the measured one.

Although a model has been proposed to predict flow power, directly measuring the flow power can be challenging. Based on the above observations, it is confirmed that the total power consumption of a piezoelectric fan is composed of power dissipation through the PZT actuator and flow power. Therefore, flow power can also be experimentally estimated by

simply deducting the measured power consumption of a PZT actuator from that of a complete piezoelectric fan. The flow power obtained by such an estimation is plotted with the predicted one in Fig. 18. As expected, they match closely.

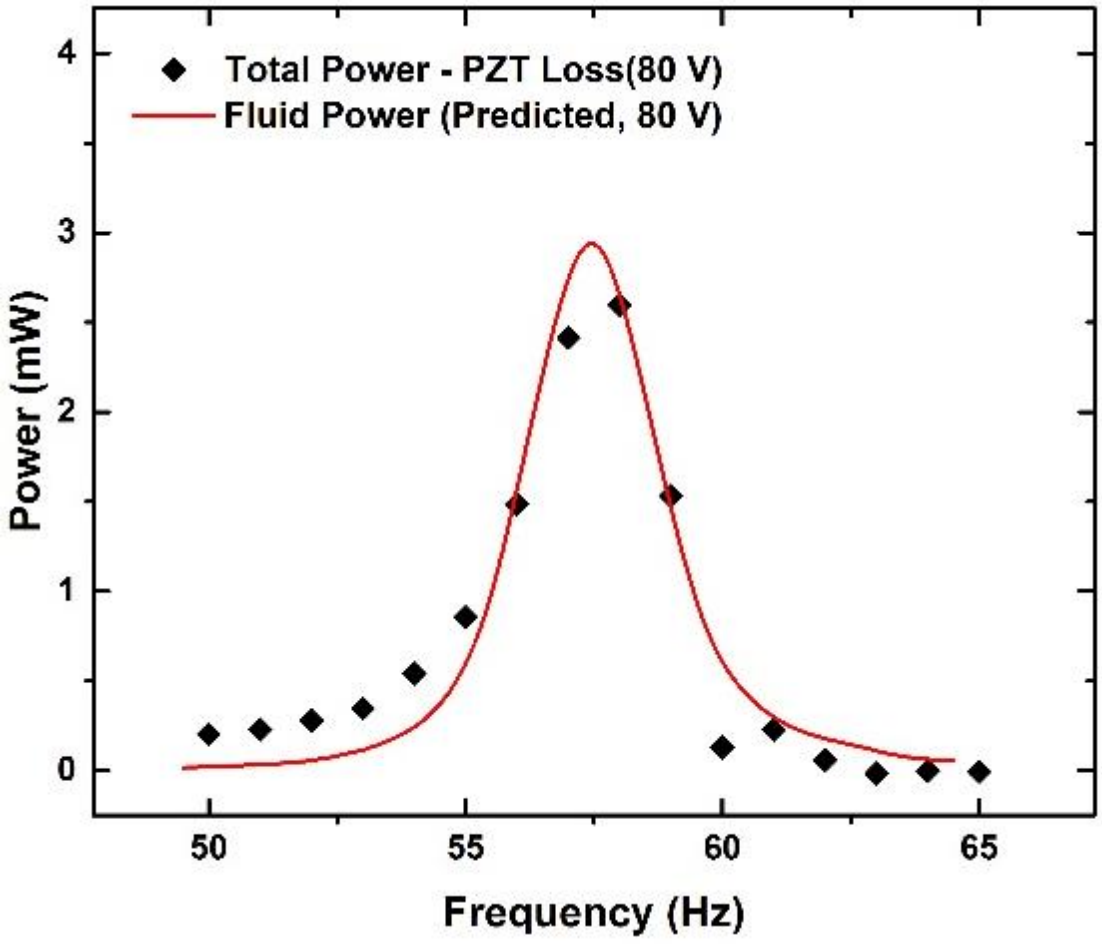

Fig. 18. Comparison between model-predicted and estimated flow power

3. Heat Transfer Analysis

Since the purpose of conducting the current research is to analyze the power efficiency of piezoelectric fan cooling, heat transfer performance needs to be thoroughly analyzed to construct an accurate model predicting efficiency. A simple rectangular shaped aluminum plate, attached by a flexible heater of the same size, is used as the heat source to avoid the effects of other factors, such as geometric dependency, complicating the analysis. Convection and radiation are believed to be the two dominant energy transfer modes analyzed in detail. The heat source is surrounded by insulation to maintain a two-dimensional analysis with assumptions of quiescent ambient air and constant heat flux.

3.1 Experimental Setup

Heat transfer experiments have been performed on a heat source made by an aluminum flat surface with a flexible heater attached to the back. The resistance of the flexible heater is measured as R_{heater} =78.5Ω. Also, the voltage of the heater is kept constant at V_{heater} =15V. Therefore, the power input of heat source can be calculated as:

$$q = \frac{V_{heater}^2}{R_{heater}} \tag{33}$$

Five type-k thermocouples are attached directly to the flat surface to measure the temperature. The average output value from all five thermocouples is used as surface temperature T_s, plugged in the previously listed equations. All temperature readings are also displayed and recorded by LabVIEW VI and output as a text file.

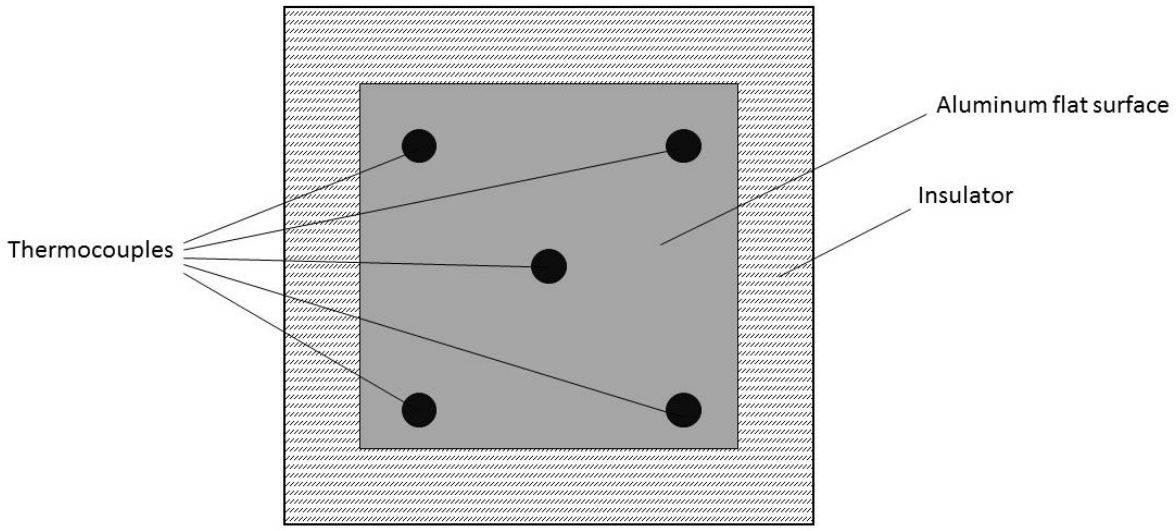

Fig.19. Heat source surface schematic

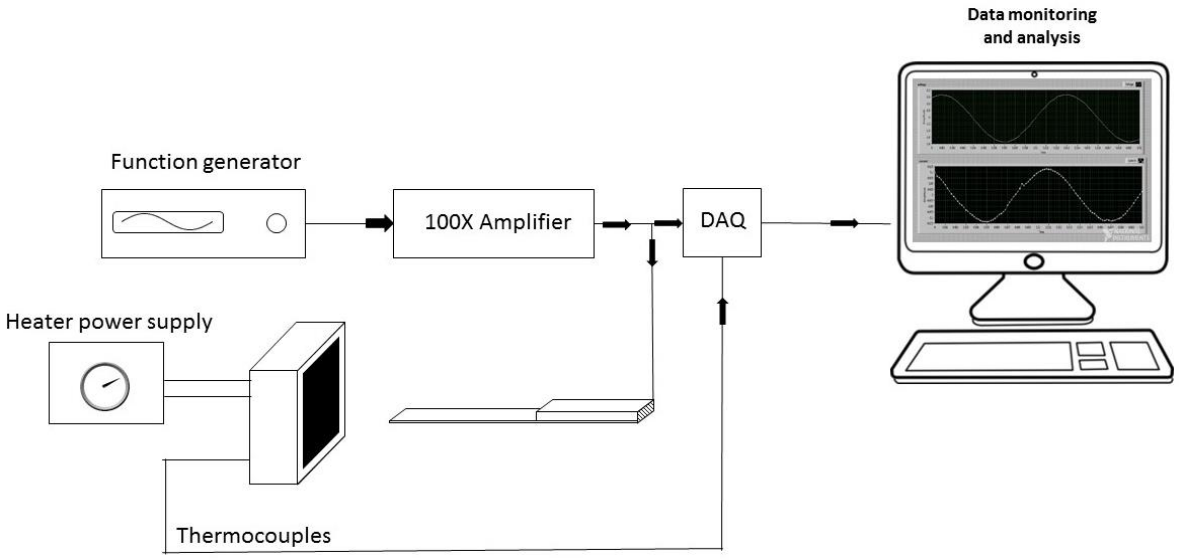

Fig.20. Complete schematic of experimental setup

3.2 Natural convection of heat source

Before the piezoelectric fan is turned on, natural convection and radiation heat transfer determine the steady state temperature. By assuming a constant heat flux, the natural convection coefficient can be obtained as follows [3]:

$$Gr^*_x = \frac{g\beta\left(\frac{q''x}{K}\right)x^3}{\upsilon^2} \tag{28}$$

$$Nu_x = 0.55(Gr^*_x Pr)^{0.2} \tag{29}$$

By utilizing a modified Grashoff number, the Nusselt number can be determined and, in turn, the natural convective heat transfer coefficient, $h_{natural\ conv}$.

$h_{natural\ conv}$ turns out to be around 15 $\frac{W}{Km^2}$.

The heat transfer coefficient should also be experimentally determined to validate the predicted one.

$$h_{total} = \frac{q_{in}}{A(T_s - T_\infty)} \tag{30}$$

At a steady state, the temperature of the heat source is around 70℃ while the room temperature is around 21℃.

However, the measured heat transfer coefficients, by varying input power, show a constant offset from predicted ones. It is confirmed that radiation needs to be included as a dominant factor.

3.3 Radiation of heat source

To control the radiation heat transfer, the heat source is sprayed with Krylon spray so that the radiation intensity can be known and fixed at 0.95. The effective radiative heat transfer coefficient can be obtained as follows:

$$h_{rad} = \epsilon\sigma(T_s^2 + T_\infty^2)(T_s + T_\infty) \tag{31}$$

h_{rad} turns out to be around 7 $\frac{W}{Km^2}$.

Before the piezoelectric fan is turned on, the heat transfer coefficient can be determined by summing up the natural convective heat transfer coefficient and the effective radiative heat transfer coefficient.

$$h_{measured\ total} = h_{rad} + h_{natural\ conv} \approx 22\ \frac{W}{Km^2} \tag{32}$$

3.4 Experimental study of power efficiency of piezoelectric fan cooling

To study the cooling performance of various piezoelectric fans normalized by their power consumptions, several experiments have been designed and conducted in which the thickness and length of the fan blade are changed. When the blade's thickness and length are changed, its resonance frequencies are also changed, leading to a change in its power consumption and cooling ability. The goal of the current study is to uncover the optimum configuration of a blade that can provide a reasonably high cooling ability and still be power efficient. The following table shows the variation of blade parameters in each experiment.

Table 1. Parameters varied in each experiment

experiment	blade length (mm)	Resonance Frequency (Hz)	Voltage (V)	Thickness (mm)
Changing Thickness	**32**	**35, 82, 96, 119**	**70, 90, 110, 140**	**0.127, 0.254, 0.371, 0.508**
Changing length	**20,21,27,31,41,49,63**	**188, 168, 122, 93, 60, 44, 30**	**70, 90, 110, 140**	**0.254**

The thickness of the blade is increased by adding additional layers of Kapton sheet, each with a thickness of 0.005".

The heat transfer enhancement by a piezoelectric fan can be estimated as:

$$h_{fan} = h_{total} - h_{natural\ conv.} \tag{34}$$

h_{fan} obtained in each experiment will then be normalized by its total power consumption and by flow power to determine its power efficiency.

$$Power\ Normalized\ Heat\ Transfer\ Coefficient\ (PNHT) \equiv \frac{h_{fan}}{P_{total}} \tag{35}$$

$$Flow\ Power\ Normalized\ Heat\ Transfer\ Coefficient\ (FPNHT) \equiv \frac{h_{fan}}{P_{flow}} \tag{36}$$

PNHT is a straightforward way to define power efficiency because it directly compares the total heat transfer coefficient gained by employing the piezoelectric fan to its total power consumption. However, as discussed in chapter two, up to half the total power is consumed by the PZT actuator that does not contribute to heat transfer enhancement. Therefore, FPNHT is used instead to characterize the power efficiency, due to its relevance to flow generation that is closely related to heat transfer enhancement. This proposed conclusion is verified by the experimental results presented below.

3.4.1 Changing thickness

Fig. 21 demonstrates the change in the fan heat transfer coefficient with increasing blade thickness. It is observed that h_{fan} reaches a maximum at a thickness of $0.01''$ (0.254 mm). It is thought that the reason for this is that, by increasing the thickness of blade, the fan possesses a higher resonance frequency, which favors the heat transfer enhancement while, on the other hand, a higher stiffness of blade is also acquired, which leads to a decrease in the vibration amplitude. Therefore, the overall interaction of the above two effects leads to an indeterminant heat transfer enhancement that requires further study to build a theoretical model predicting optimization.

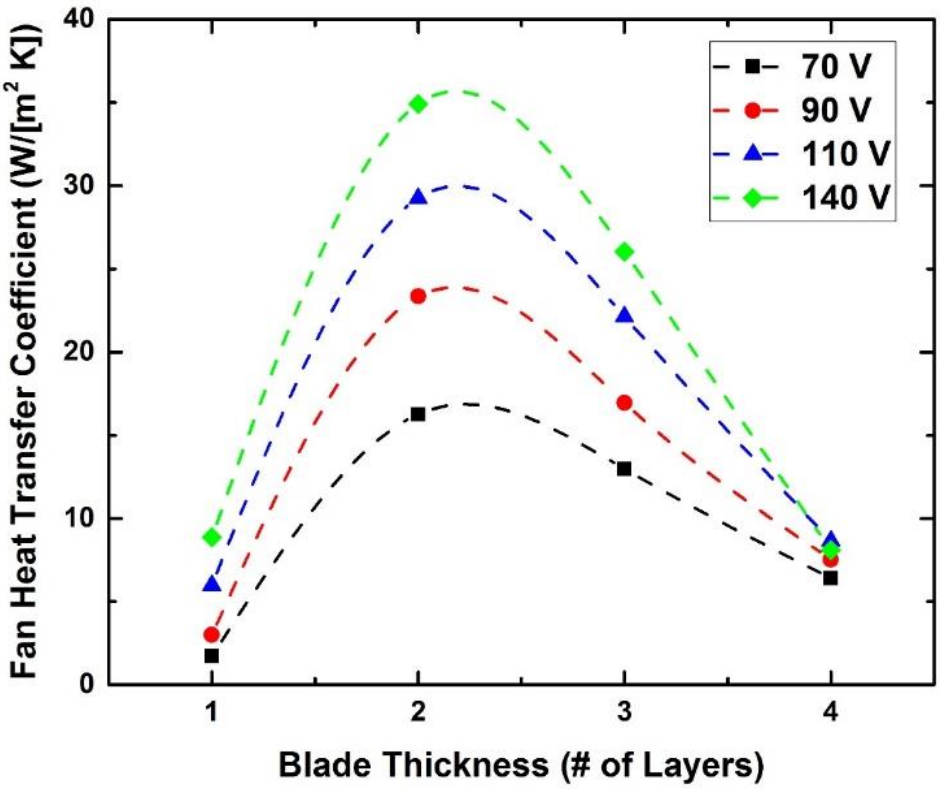

Fig.21. Fan heat transfer coefficient of different blade thicknesses under various input voltage

(a)

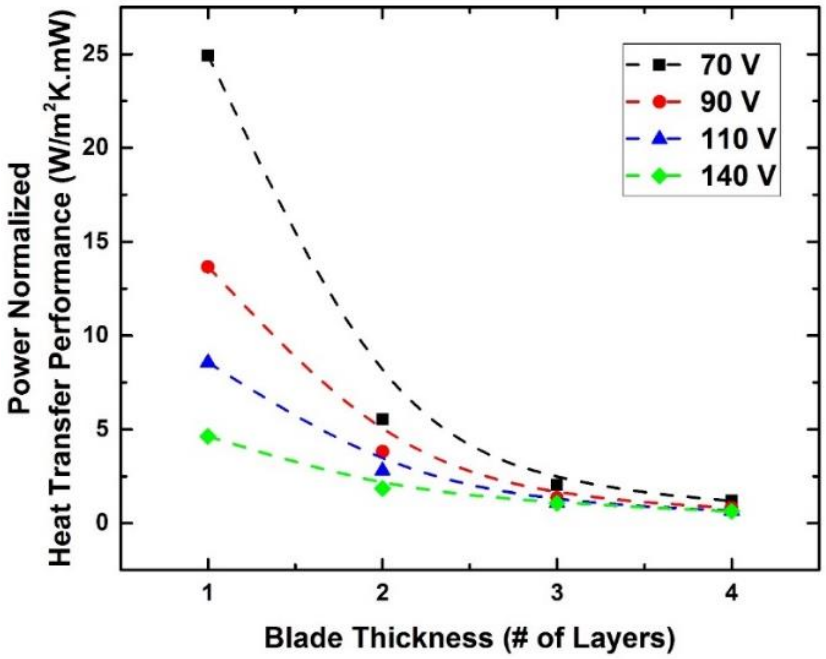

(b)

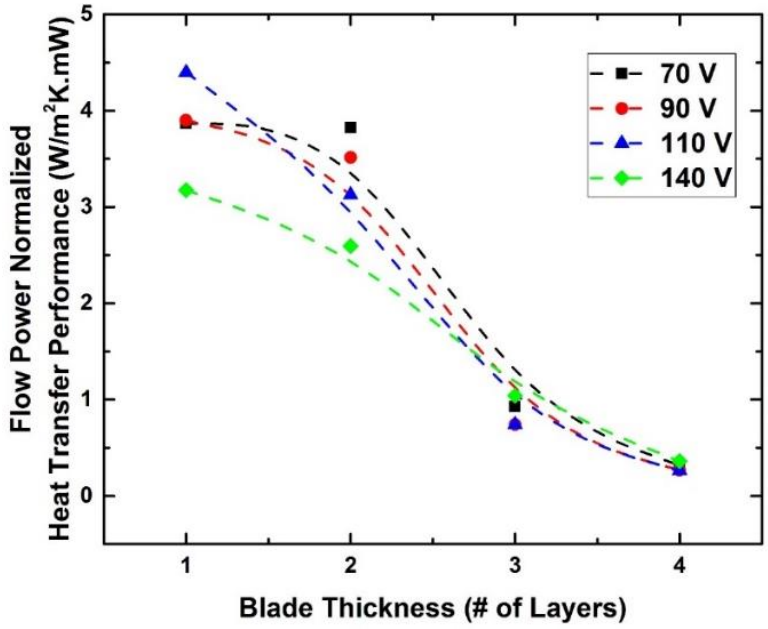

Fig.22. (a) PNHT (b)FPNHT of a piezoelectric fan with different blade thickness under various input voltages

As shown in Fig. 22, under different input voltages, the PNHT diverges drastically when the blade is thin, while the FPNHT follows a similar curve as input voltages change. When the blade is thin, the resonance frequency is low. As seen from chapter two, the power consumed by a PZT actuator increases linearly with frequency. Therefore, at a lower resonance frequency, a larger portion of the total input power transfers to the surrounding air, leading to higher power efficiency. By excluding the power consumption of a PZT actuator, the power efficiency seems to be independent of input voltages.

3.4.2 Changing Length

In the following set of experiments, the blade length is changed to obtain different resonance frequencies. Blades with seven different lengths have been tested. Fig. 23 shows fan heat transfer coefficient vs. blade lengths. It is observed that elongating the fan blade tends to decrease the heat transfer enhancement, due to a low resonance frequency generating a weak air flow, despite the large vibration amplitude associated with it. However, a short blade, due to its extremely small vibration amplitude, also has a small heat transfer coefficient. Thus, there is an optimum value for blade length that requires further study to be theoretically identified.

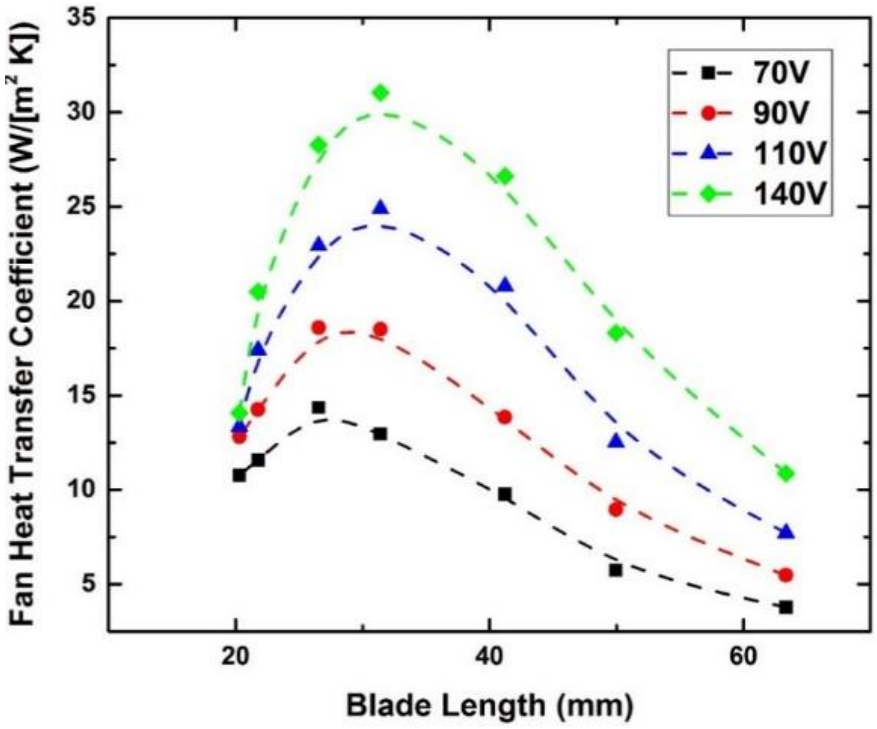

Fig.23. Fan heat transfer coefficient of different blade lengths under various input voltage

(a)

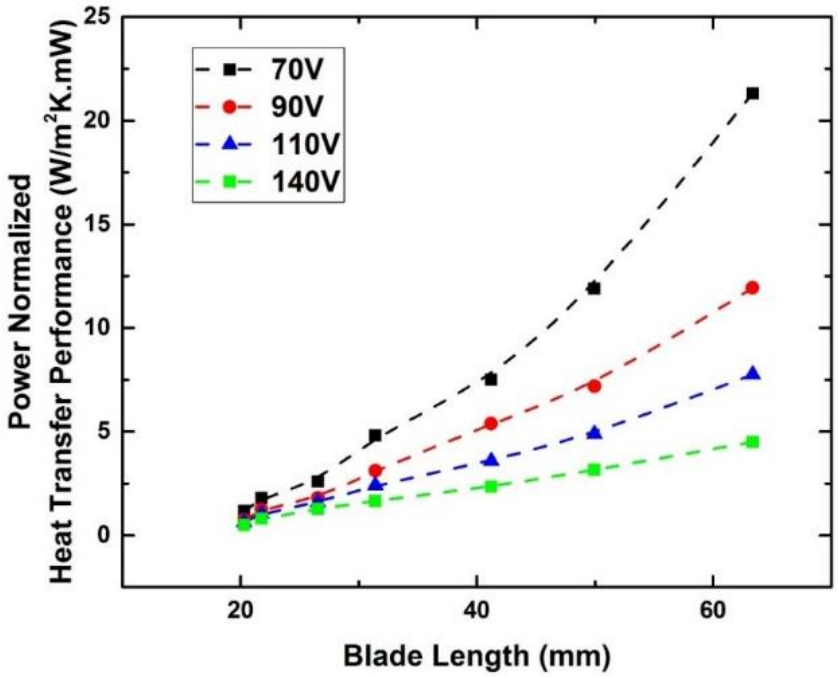

(b)

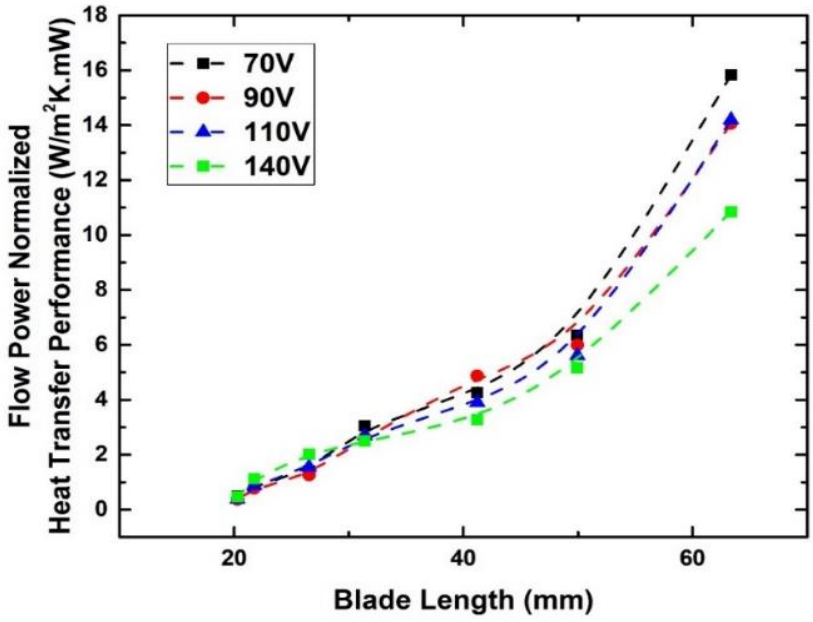

Fig.24. (a) PNHT (b)FPNHT of a piezoelectric fan with different blade lengths under various input voltages

As demonstrated in Fig. 24, the power efficiency of a piezoelectric fan increases as its blade length increases due to the low resonance frequency of a long blade. Like fans with different blade thicknesses, FPNHT follows a unified curve that increases with decreasing resonance frequencies and is independent of input voltages, indicating the fact that, when determining the power efficiency of a piezoelectric fan, the flow power is a critical factor to be taken into consideration. However, when choosing a piezoelectric fan for a particular application, the fan heat transfer coefficient should also be kept in mind as an extremely low fan heat transfer coefficient is observed at a blade length of 60 mm, the power efficiency of which can be ten times higher than that of a blade length of 20 mm. The balance between high power efficiency and reasonable heat transfer enhancement serves as an important criterion when making or selecting piezoelectric fans.

4. Conclusion and Future Work

Due to lack of systematic study in detailed power consumption prediction of piezoelectric fan, the current work proposed an analytical model, Eqn.26, to partition the input driving power into the mechanical dissipation of the PZT actuator and the induced flow power of the surrounding air. Knowing partitioned power consumption and experimentally obtaining cooling enhancement, the power efficiency of piezoelectric fan cooling is then defined as forced heat transfer coefficient normalized by flow power. Instead of solely focusing on cooling enhancement, the current work offers a new perspective in evaluating piezoelectric fan's performance by acquiring its power efficiency, where experimentally obtained heat transfer coefficient is normalized by analytically estimated flow power.

When developing the analytical model, considering the mechanical dissipation of the PZT actuator, including the effect of hysteresis loss and mechanical damping, a modified EOM is utilized. However, since the EOM is a non-linear second order differential equation, obtaining an analytical solution can be complicated. Therefore, curve fittings based on experimentally measured vibration amplitudes are utilized to obtain key parameters such as a damping coefficient to estimate a PZT actuator's power dissipation. A similar approach is adopted to estimate the flow power. By curve fitting the vibration amplitude of fan blade, the key parameter, aerodynamic damping coefficient, is obtained and, in turn, the flow power.

The power consumptions of a piezoelectric fan and a PZT actuator are measured to experimentally verify the validity of the models mentioned above. The model-predicted power dissipation of PZT actuator is shown to match that measured in both trend and magnitude. It is also observed that the difference between the power consumption of a PZT

actuator and that of a complete piezoelectric fan is close to the predicted flow power. Therefore, the flow power can be experimentally obtained by subtracting the measured power consumption of a PZT actuator from that of a complete piezoelectric fan.

The heat transfer performance of piezoelectric fans, in terms of heat transfer enhancement, is studied with fans whose blades are of differing length and thickness. By normalizing the heat transfer coefficient with the corresponding flow power, the power efficiency of a piezoelectric fan operating under various input bias voltages follows a similar trend. When selecting a specific type of piezoelectric fan for a cooling application, both heat transfer performance and power efficiency should be evaluated simultaneously to ensure the desired outcome is achieved.

As for future work, as it is observed from heat transfer experiments where thickness and length of blade are changed that the cooling enhancement peaks with the fan blade having a particular bending stiffness. A stiff blade has a high resonance frequency and low vibration amplitude while opposite combination is found for soft blade. By adjusting the stiffness of blade, its vibration induced vortex strength is varied, providing different heat transfer enhancement. Therefore, the optimization of piezoelectric fan's cooling enhancement by adjusting blade's bending stiffness needs to be further studied.

Based on piezoelectric fan's power partitioning, discussed in chapter two, as much as half of the total power input is consumed by PZT actuator, which does not contribute to heat transfer enhancement. Therefore, another potential topic for future study can lie in discovering different combination of actuator and fan blade to achieve better power efficiency in terms of having higher percentage of input power converted into flow power compared to that of currently available ones.

References

[1] J. H. Yoo, J. I. Hong, and W. Cao, “Piezoelectric ceramic bimorph coupled to thin metal plate as cooling fan for electronic devices,” *Sens. Actuators Phys.*, vol. 79, no. 1, pp. 8–12, Jan. 2000.

[2] M. Arik, J. Petroski, A. Bar-Cohen, and M. Demiroglu, “Energy Efficiency of Low Form Factor Cooling Devices,” pp. 1347–1354, Jan. 2007.

[3] T. Açıkalın, S. V. Garimella, A. Raman, and J. Petroski, “Characterization and optimization of the thermal performance of miniature piezoelectric fans,” *Int. J. Heat Fluid Flow*, vol. 28, no. 4, pp. 806–820, Aug. 2007.

[4] “Phase-resolved flow field produced by a vibrating cantilever plate between two endplates,” *Phys. Fluids*, vol. 16, no. 1, pp. 145–162, Dec. 2003.

[5] A. Eastman, J. Kiefer, and M. Kimber, “Thrust measurements and flow field analysis of a piezoelectrically actuated oscillating cantilever,” *Exp. Fluids*, vol. 53, no. 5, pp. 1533–1543, Nov. 2012.

[6] T. Acikalin, S. Wait, S. Garimella, and A. Raman, “Experimental Investigation of the Thermal Performance of Piezoelectric Fans,” *CTRC Res. Publ.*, Jan. 2004.

[7] M. Kimber, S. V. Garimella, and A. Raman, “An Experimental Study of Fluidic Coupling Between Multiple Piezoelectric Fans,” in *Thermal and Thermomechanical Proceedings 10th Intersociety Conference on Phenomena in Electronics Systems, 2006. ITHERM 2006.*, 2006, pp. 333–340.

[8] S. M. Wait, S. Basak, S. V. Garimella, and A. Raman, “Piezoelectric Fans Using Higher Flexural Modes for Electronics Cooling Applications,” *IEEE Trans. Compon. Packag. Technol.*, vol. 30, no. 1, pp. 119–128, Mar. 2007.

[9] C. Liang, F. P. Sun, and C. A. Rogers, “An Impedance Method for Dynamic Analysis of Active Material Systems,” *J. Intell. Mater. Syst. Struct.*, vol. 8, no. 4, pp. 323–334, Apr. 1997.

[10] Y. S. Cho, Y. E. Pak, C. S. Han, and S. K. Ha, “Five-port equivalent electric circuit of piezoelectric bimorph beam,” *Sens. Actuators Phys.*, vol. 84, no. 1–2, pp. 140–148, Aug. 2000.

[11] W.-J. Sheu, R.-T. Huang, and C.-C. Wang, “Influence of bonding glues on the vibration of piezoelectric fans,” *Sens. Actuators Phys.*, vol. 148, no. 1, pp. 115–121, Nov. 2008.

[12] “IEEE Standard on Piezoelectricity,” *ANSIIEEE Std 176-1987*, p. 0_1-, 1988.

[13] K. Yao and K. Uchino, “Analysis on a composite cantilever beam coupling a piezoelectric bimorph to an elastic blade,” *Sens. Actuators Phys.*, vol. 89, no. 3, pp. 215–221, Apr. 2001.

[14] T. S. Low and W. Guo, “Modeling of a three-layer piezoelectric bimorph beam with hysteresis,” *J. Microelectromechanical Syst.*, vol. 4, no. 4, pp. 230–237, Dec. 1995.

[15] M. Toda, “Theory of air flow generation by a resonant type PVF2 bimorph cantilever vibrator,” *Ferroelectrics*, vol. 22, no. 1, pp. 911–918, Jan. 1978.

[16] M. L. James, Ed., *Vibration of mechanical and structural systems: with microcomputer applications*, 2nd ed. New York, NY: HarperCollins College Publishers, 1994.

[17] “LabVIEW System Design Software - National Instruments.” [Online]. Available: http://www.ni.com/labview/. [Accessed: 09-Mar-2017].

[18] “MATLAB - MathWorks.” [Online]. Available: https://www.mathworks.com/products/matlab.html. [Accessed: 09-Mar-2017].

[19] “ImageJ.” [Online]. Available: https://imagej.nih.gov/ij/. [Accessed: 09-Mar-2017].

[20] D. Whitley, “A genetic algorithm tutorial,” *Stat. Comput.*, vol. 4, no. 2, pp. 65–85, Jun. 1994.

[21] H. Matthew W., “Properties of PZT-Based Piezoelectric Ceramics Between 150 and 250 Degrees Celcius,” NASA Langley Technical Report Server, 1998.

[22] A. I. Kingon, P. J. Terblanche, and J. B. Clark, “Variability of the high field properties of PZT-4 and PZT-8 type piezoelectric ceramics,” *Ferroelectrics*, vol. 37, no. 1, pp. 635–638, Oct. 1981.